Bioresource Technology 311 (2020) 123538

Contents lists available at ScienceDirect

Bioresource Technology

journal homepage: www.elsevier.com/locate/biortech

Enhanced P450 fatty acid decarboxylase catalysis by glucose oxidase coupling and co-assembly for biofuel generation

Libo Zhang[a], Olivia M. Manley[a], Dumei Ma[a,b], Yingwu Yin[b], Thomas M. Makris[a], Qian Wang[a,*]

[a] Department of Chemistry and Biochemistry, University of South Carolina, 631 Sumter Street, Columbia, SC 29208, USA
[b] Department of Chemical and Biochemical Engineering, College of Chemistry and Chemical Engineering, Xiamen University, Xiamen 361005, Fujian, China

ARTICLE INFO

Keywords:
P450 OleT
Glucose oxidase
Enhanced activity
Enzyme cascade
Co-assembly
Terminal alkenes

ABSTRACT

Cytochrome P450 OleT is a fatty acid decarboxylase that uses hydrogen peroxide (H_2O_2) to catalyze the production of terminal alkenes, which are industrially important chemicals with biofuel and synthetic applications. Despite its requirement for large turnover levels, high concentrations of H_2O_2 may cause heme group degradation, diminishing enzymatic activity and limiting broad application for synthesis. Here, we report an artificial enzyme cascade composed of glucose oxidase (GOx) and $OleT_{SA}$ from *Staphylococcus aureus* for efficient terminal alkene production. By adjusting the ratio of GOx to $OleT_{SA}$, the GOx-based tandem catalysis shows significantly improved product yield compared to the H_2O_2 injection method. Moreover, the co-assembly of the GOx/$OleT_{SA}$ enzymes with a polymer, forming polymer-dual enzymes nanoparticles, displays improved activity compared to the free enzyme. This dual strategy provides a simple and efficient system to transform a naturally abundant feedstock to industrially important chemicals.

1. Introduction

Driven by the shortage of fossil fuel reserves and increasing environmental concerns, tremendous efforts have been undertaken to transform bio-based feedstock into chemicals (Corma et al., 2007; Bhatia et al., 2019) and fuels (Potocnik, 2007; Mateo et al., 2020). Among them, the conversion of bioavailable carboxylic acids (e.g., fatty acids) into terminal alkenes attracts attention because of their applications as next-generation fuels and key chemicals for the production of lubricants, surfactants, detergents, plastics, etc (Peralta-Yahya et al., 2012; Ray et al., 2012; Lane and Burgess, 2001). To achieve this goal, different methodologies have been developed such as esterification, amidation (Aransiola et al., 2014) and chemical reductions (Das et al., 2012). Despite of the success of these methods, the requirement of precious transition metal catalysts and the harsh reaction conditions often raise environmental concerns. Therefore, enzyme-catalyzed oxidative decarboxylation reactions that can directly produce terminal alkenes in mild conditions provide viable alternative approaches (Dennig et al., 2016; Lu et al., 2018).

A promising enzymatic alternative, cytochrome P450 OleT from *Jeotgalicoccus* sp. 8456, was first identified as an efficient olefin producer by Rude and coworkers (Rude et al., 2011). OleT catalyzes the oxidative decarboxylation of fatty acids to yield primarily terminal alkenes and CO_2 or minor α- and β-hydroxylated fatty acids side-products (Grant et al., 2015; Rude et al., 2011). Whereas the majority of P450s activate atmospheric O_2 using pyridine dinucleotide as a reducing source and an auxiliary redox chain (Munro et al., 2018), the OleT enzyme utilizes H_2O_2 as the only electron- and oxygen-source throughout the catalytic cycle (Fig. 1**a**) (Wise et al., 2018). Unlike NAD(P)H, H_2O_2 is inexpensive and easily scalable, and previous efforts have sought to rewire P450s for efficient peroxide utilization (Joo et al., 1999). However, the low turnover rate and low stability in the presence of excess H_2O_2 limit the practical use of OleT. Very recently, a functional ortholog from *Staphylococcus aureus,* $OleT_{SA}$ (Amaya, 2018; Jiang et al., 2019), was characterized by us and others that possesses improved features including enhanced solubility and high stability. These features enable this ortholog to be a promising candidate for production applications.

One major issue of the H_2O_2-dependent biocatalysts towards their industrial applications is enzyme inactivation (Burek et al., 2019). High concentrations of peroxide will generally oxidize some key amino acids (e.g. methionine) in the vicinity of enzyme active site (Ogola et al., 2010) or directly destroy the porphyrin cofactor, resulting in bleaching of the heme (Ayala et al., 2011). To alleviate this issue, controlling the concentration of peroxide during the catalytic reactions by employing *in situ* generation techniques provides a facile way to reduce the peroxide-related enzyme inactivation (Amaya et al., 2016; Burek et al., 2019). To date, photochemical and biological approaches that generate

* Corresponding author.
E-mail address: wang263@mailbox.sc.edu (Q. Wang).

https://doi.org/10.1016/j.biortech.2020.123538
Received 6 April 2020; Received in revised form 11 May 2020; Accepted 12 May 2020
Available online 15 May 2020
0960-8524/

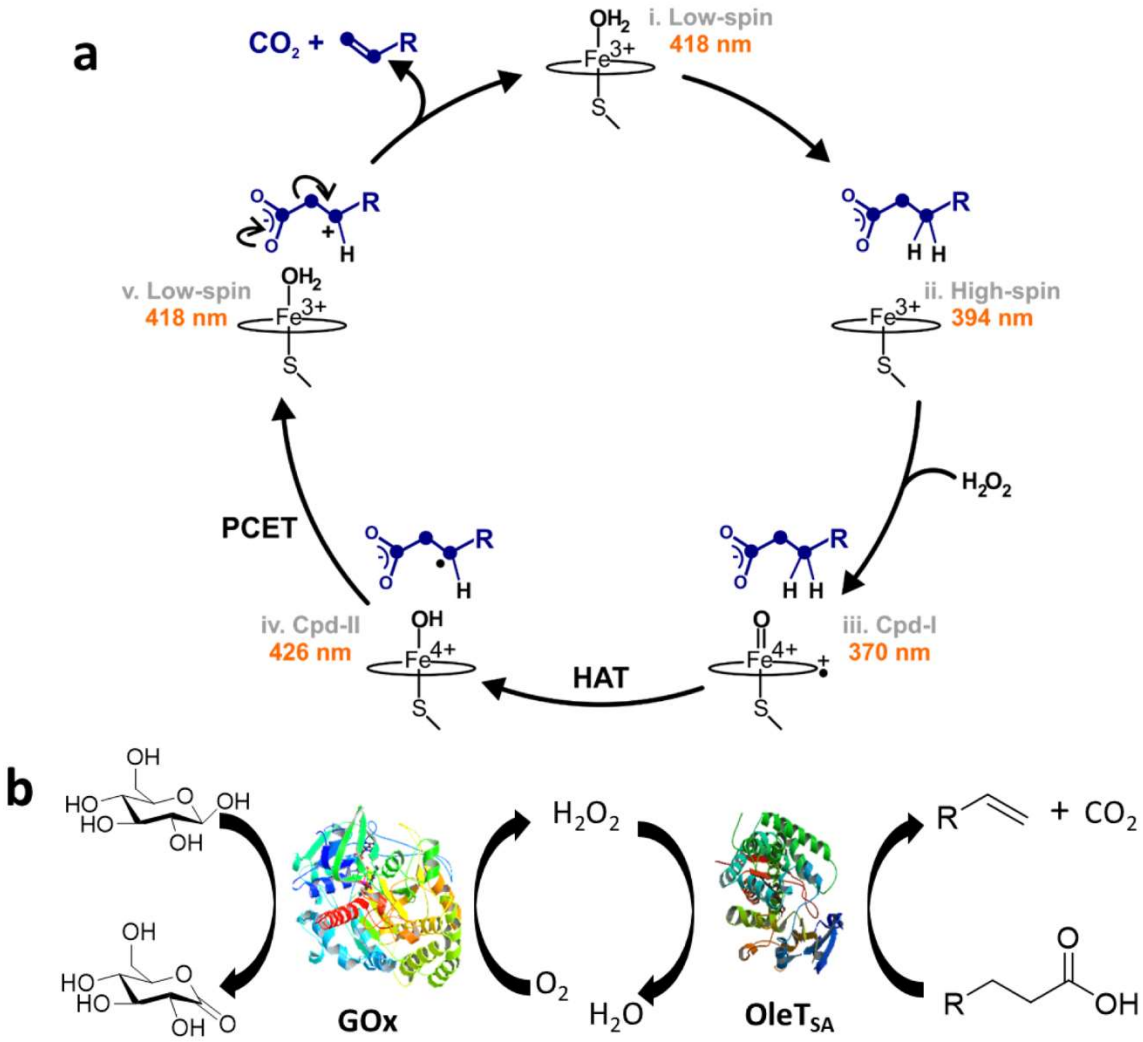

Fig. 1. (a) Scheme of the cytochrome P450 OleT enzyme catalytic cycle. OleT is in a low-spin ferric resting state with its heme iron axially coordinated by cysteine thiolate and a H_2O molecule, which shows a maximum Soret band at 418 nm (Munro et al., 2018). Substrate binding displaces the axial water and converts the heme iron from low-spin to a high-spin state with a maximum Soret band at 394 nm (Munro et al., 2018). Subsequent H_2O_2 activation forms Compound I (Grant et al., 2015), which abstracts a hydrogen atom from the C_β position (HAT step), resulting in formation of a substrate radical and the Fe^{4+}-hydroxo species (compound II) (Grant et al., 2016). Further substrate oxidation, and recruitment of a proton results in the elimination of CO_2 (PCET step) and terminal alkene formation. (b) Schematic representation of GOx/OleTSA cascade using glucose as a substrate to produce H_2O_2 *in situ*.

H_2O_2 in a controlled manner have been reported to leverage OleT enzyme catalysis. Zachos and colleagues described an *in situ* H_2O_2-generation system that uses light to excite flavin cofactors with ethylenediaminetetraacetic acid (EDTA) as an electron donor, which converts dioxygen to H_2O_2 to active the $OleT_{JE}$ enzyme for terminal alkenes production (Zachos et al., 2015). Matthews *et al.* reported an enzyme genetic fusion system in which $OleT_{JE}$ was linked to alditol oxidase (AldO). With this system, polyol substrates were fed as AldO substrates to generate H_2O_2 (Matthews et al., 2017). While the overall design is very innovative, the low expression level of the recombinant protein and the fixed ratio of the two enzymes may limit its applications. Some H_2O_2-independent methods were reported to employ the O_2 activating pathway to active OleT catalysis for alkene production (Liu et al., 2014). While it represents a very interesting reaction pathway (Wise et al., 2018), the usage of expensive reducing sources (e.g. NADH, NADPH) and redox partners limit their synthetic applications in vitro. On the other hand, these initial investigations inspired us to explore more simple and efficient *in situ* H_2O_2-generation methods to improve $OleT_{SA}$ catalysis for biofuel production.

In this work, we report the use of glucose oxidase (GOx) and sugars as substrates to efficiently drive $OleT_{SA}$ catalysis in an adjustable manner (Fig. 1**b**). GOx is a flavoenzyme that metabolizes $_D$-glucose by using molecular oxygen as an electron acceptor with simultaneous production of H_2O_2 (Wilson and Turner, 1992). GOx is widely used in food, textile, and glucose-sensing industries because of its high stability and catalytic efficiency (Bankar et al., 2009). Other substrates of GOx include $_D$-mannose, $_D$-galactose and $_D$-xylose (Adams et al., 1960), which are all abundant and renewable feedstocks. Moreover, GOx has significantly varied kinetics with different substrates (Gibson et al., 1964), which enables one to regulate the H_2O_2-generating process. The data presented in this manuscript demonstrates improved catalytic efficiency of OleT enzyme when coupled with the GOx enzyme (the GOx method) compared to a single injection of H_2O_2 (the H_2O_2 method). In addition, we use a poly(4-vinylpyridine) (P4VP) polymer to co-assemble GOx and $OleT_{SA}$ enzymes to generate nanoparticles (NPs) in order to further optimize the catalytic efficiency of enzyme cascade. The combination of the GOx-based method and the dual enzyme co-assembly with polymers provides a novel way to leverage OleT enzyme catalysis, which can be potentially used for synthetic applications.

2. Materials and methods

2.1. Materials

GOx from *Aspergillus niger* and H_2O_2 were purchased from Sigma. Eicosanoic acid (C20:0), stearic acid (C18:0), palmitic acid (C16:0), myristic acid (C14:0), lauric acid (C12:0), and capric acid (C10:0) were purchased from BDH Chemicals. The alkene standard 1-hexadecene was purchased from TCI chemicals. D-Glucose, D-mannose, D-galactose were purchased from Fisher. Hydrocinnamic acid and P4VP (Mw 60000) were purchased from Sigma-Aldrich. *N,O*-Bis(trimethylsilyl)trifluoroacetamide (BSTFA)/trimethylchlorosilane (TMCS) (99:1) were purchased from Supelco (Bellefonte, PA, USA). Unless otherwise noted, all chemicals and solvents used were of analytical grade and were used as received from commercial sources. Unless otherwise noted, 200 mM K_2HPO_4, 100 mM NaCl, pH 7.4 was used as buffer.

2.2. Methods

2.2.1. Heterologous expression and purification of $OleT_{SA}$

The original $OleT_{SA}$ gene was synthesized by Bio Basic Inc. (Markham, Ontario). The gene was subcloned onto a kanamycin-resistant T5 plasmid pJ401containing a C-terminal HisTag. The construct was transformed into BL21(DE3) containing the pTF2 plasmid encoding for GroEL/GroES/Tig onto a kanamycin (50 μg/mL)/chloramphenicol (30 μg/mL) LB plate. Kanamycin (50 μg/mL) and chloramphenicol (20 μg/mL) were used to grow a cell culture in Modified Terrific Broth (TB). For protein expression, 10 mL of this starter culture was used to inoculate 500 mL of TB containing 50 μg/mL kanamycin, 30 μg/mL chloramphenicol, 125 mg/L thiamine, and trace metals (Amaya, 2018). The cultures were grown to an $OD_{600\ nm}$ of 1.0, at which point protein expression was induced with 100 μM IPTG, 10 ng/mL tetracycline and 10 mg/L of 5-aminolevulinic acid. The culture was incubated at 18 °C for an additional 16–18 h and harvested by centrifugation for purification or for storage at −80 °C until further use. The protein was purified using nickel-nitriloacetic acid (Ni-NTA) affinity chromatography followed by Butyl-S-Sepharose column purification as described previously (Amaya, 2018). Fractions with an R_z value ($Abs_{418\ nm}$/$Abs_{280\ nm}$) above 1.2 were pooled and dialyzed against 200 mM KPi pH 8. Proteins were stored at −80 °C until further use.

2.2.2. $OleT_{SA}$ enzyme activity assays

Eicosanoic acid and stearic acid stock (10 mM) were dissolved in 70% ethanol/30% Triton X-100 (unless otherwise noted) as stocks. Other fatty acids including palmitic acid, myristic acid and lauric acid were dissolved in DMSO to make 10 mM stocks. Hydrocinnamic acid was dissolved in DMSO to make a 400 mM stock. To set up enzymatic reactions, 5 μM $OleT_{SA}$, 500 μM or 1 mM fatty acids or 1 mM hydrocinnamic acid (unless otherwise noted) from above stocks were used for multiple-turnover reactions in a 150 μL volume. H_2O_2 was added at a concentration of 2 mM to initiate the reactions in H_2O_2 method, while 10 nM to 5 μM GOx was added to initiate the reactions in GOx method. D-glucose, D-mannose, or D-galactose (6.6 mM) were used in the GOx method unless otherwise noted. An exponential model was used to fit the progress of the steady-state reactions to highlight the different enzyme kinetics with different methods. Duplicate experiments for each reaction were done. The reactions were quenched with 0.4 mM HCl or 1% acetic acid for GC/GC–MS or LC/LC-MS analysis, respectively.

2.2.3. Heme decay monitoring

Heme decay was monitored with UV–Visible spectroscopy on an HP 8453 spectrophotometer. A quartz cuvette with 1 cm path length was used. For the heme decay monitoring during GOx- or H_2O_2-driven reactions, 5 μM $OleT_{SA}$, 0.5 mM eicosanoic acid in the presence of 2 mM H_2O_2 or 10 nM GOx and 6.6 mM glucose were used. $OleT_{SA}$ spectra were recorded over time for 1 h at room temperature. Active enzyme concentration was determined from the total thiolate-ligated heme in the sample, based on the extinction coefficients of the Soret peaks: at 418 nm, 112.8 $mM^{-1}cm^{-1}$ for low-spin fraction, 56.6 $mM^{-1}cm^{-1}$ for high-spin fraction; 86.8 $mM^{-1}cm^{-1}$ at 406 nm; at 394 nm, 50 $mM^{-1}cm^{-1}$ for low-spin fraction, 106.5 $mM^{-1}cm^{-1}$ for high-spin fraction (Amaya, 2018).

2.2.4. Gas chromatography (GC) analysis

For gas chromatographic quantification of fatty acid metabolism by $OleT_{SA}$, internal standards including 1-hexadecene and a C_{n-2} fatty acid (relative to substrate of chain-length C_n) were added after the reactions were quenched with 300 mM HCl. The reactions were extracted with 300 μL chloroform. The organic phases of each reaction were tested on GC directly or derivatized before GC analysis. For derivatization, samples were concentrated under a stream of N_2 gas to less than 50 μL, then derivatized with 250 M equivalents of BSTFA:TMCS (99:1). Samples were incubated at 60 °C for 20 min for trimethylsilylation. Following the derivatization, samples were analyzed by GC. The following oven conditions were used to detect products of C20 through C16 fatty acids: 170 °C for 3 min, 10 °C/min to 220 °C, 5 °C/min to 320 °C, and 320 °C for 3 min. The following oven conditions were used to detect products of C14 and C12 fatty acids metabolism: 100 °C for 3 min, 5 °C/min to 250 °C and 250 °C for 3 min. The response factors between fatty acids, hydroxyl fatty acids and alkenes were determined by analyzing known authentic fatty acids (C18-C10) and 1-hexadecene standards.

2.2.5. HPLC and MS analysis

Reactions (total volume = 150 μL) with hydrocinnamic acid were quenched by acetic acid (final concentration 1% v/v). After quenching, 1,2,3,4-tetramethyl benzene was added as internal control and the mixture was extracted with ethyl acetate (300 μL). For each sample, 20 μL of organic layer was were injected in an Agilent 1100 HPLC equipped with a ZORBAX SB-C18 column. HPLC parameters were as follows: 25 °C; solvent A, 1% acetic acid in water; solvent B, methanol; gradient, 10% B for 2 min; then, from 10% B to 100% B over 32 min; then, from 100% B to 10% B over 10 min, flow rate, 0.5 mL/min. Detection of the products was by UV absorbance at 250 nm. Quantification of product was calculated from a calibration curve of styrene with the same extraction method. The identity of the styrene product was confirmed by GC–MS at the Mass Spectrometry Center, University of South Carolina.

2.2.6. Synthesis of P4VP-GOx-OleT assemblies

A solution of P4VP in ethanol (2.5 $mg{\cdot}mL^{-1}$, 0.1 mL) was slowly added to a solution containing 1 μM $OleT_{SA}$ and 1 μM GOx in buffer A (0.9 mL) with stirring. After addition, the mixture was stirred for an additional 10 min for equilibration. Because of the high loading capacity (Suthiwangcharoen et al., 2014), the co-assemblies was not purified before characterization and activity test.

2.2.7. Activity comparison of P4VP-GOx-$OleT_{SA}$ assemblies and free GOx/$OleT_{SA}$ enzyme cascade

The activities of both P4VP-GOx-$OleT_{SA}$ and free enzyme cascade were assessed in a reaction volume of 250 μL containing GOx and $OleT_{SA}$ (1 μM/each), hydrocinnamic acid (2 mM) or myristic acid (1 mM). Reactions were initiated by the addition of mannose (6.6 mM) to the reaction mixture and incubated at room temperature (23–25 °C). In the control reactions, GOx and mannose were omitted from the reaction sample and instead, 2 mM H_2O_2 was used to initiate the reactions. A stock solution of 400 mM hydrocinnamic acid was prepared in DMSO. The final organic solvent concentration in the reaction is 9.2% ethanol and 1% DMSO for each sample. The reaction was quenched by the addition of 1% acetic acid, and an internal standard of 1,2,3,4-tetramethyl benzene was added. The products were extracted with 300 μL ethyl acetate and analyzed by LC or GC as described above. An exponential model was used to fit the progress of the steady-state

reactions. Duplicate experiments for each reaction were done.

2.2.8. Catalase competition assay

Catalase, as a scavenger for H_2O_2, was added to the enzymatic reactions catalyzed by assembled enzyme cascade (P4VP-GOx-OleT_{SA}) and free GOx/OleT_{SA} to measure the differences. A serial concentration of catalase from 15.6 nM to 250 nM was added into the reaction mixtures containing GOx and OleT_{SA} (1 μM/each), hydrocinnamic acid (2 mM), and mannose (6.6 mM). As above, the reactions were initiated by the addition of mannose and quenched by the addition of 1% acetic acid, and 1,2,3,4-tetramethyl benzene was added as internal standard. The reactions were extracted by 300 μL ethyl acetate and analyzed by LC.

3. Results and discussion

3.1. H_2O_2 concentration dependence of OleT_{SA} activity and heme bleaching

As shown in Fig. 1**a,** a certain level of H_2O_2 is necessary to drive OleT enzymatic catalysis to form oxidizing species known as Compound I. However, with excess H_2O_2, the enzyme displays low substrate conversion (Amaya et al., 2016; Rude et al., 2011), suggesting peroxide-mediated enzyme inactivation. To characterize the H_2O_2 concentration dependence of OleT_{SA} enzymatic activity, varying concentrations of H_2O_2 were added in the enzyme reaction with eicosanoic acid as the substrate. Nonadecene production (which is the sole product of eicosanoic acid reaction) (Amaya, 2018) was used to calculate the product conversion rate. As shown in Fig. 2**a**, with increasing H_2O_2 concentration from 0.05 mM to 2 mM, increased conversions from 4% to 12% were obtained. On the other hand, increasing the H_2O_2 concentration further from 2 mM to 40 mM led to a decreased conversion. A similar trend was also observed for OleT_{SA}-catalyzed styrene production using hydrocinnamic acid as substrate. These results demonstrate that the H_2O_2 concentration has a dramatic effect on OleT_{SA} catalytic efficiency.

The destruction of the heme group of P450s and unspecific peroxygenases by H_2O_2 or other reactive intermediates such as superoxide anion (O^{2-}) and hydroxyl radical (˙OH) has been widely reported (Karuzina and Archakov, 1994; Vidal-Limón et al., 2013). Because the intact heme has prominent optical features, heme degradation can be easily monitored by the loss of these features (Karich et al., 2016). In the low-spin ferric resting state, the most intense optical peak of P450s is the Soret band, which is centered at 418 nm for substrate-free low-spin OleT_{SA} (Amaya, 2018). Upon the injection of increasing concentrations of H_2O_2 from 0.05 mM to 40 mM, the Soret band absorption of OleT_{SA} decreases, implying heme destruction with H_2O_2 treatment. More serious heme bleaching and protein precipitation occurs upon longer incubation with high concentration of H_2O_2. Even with 2 mM H_2O_2, a condition in which the enzyme shows maximized conversion rate (Fig. 2a), significant heme bleaching can be observed over time. These results suggest that heme destruction is a key factor that limits OleT_{SA} catalysis, and thus maintaining a compatible H_2O_2 concentration during the reaction could potentially improve OleT_{SA} catalytic efficiency. Slow H_2O_2 perfusion or fed-batch method have been used to circumvent the heme issue (Amaya et al., 2016; Jiang et al., 2019). In this contribution, we propose to use a GOx enzyme-based *in situ* H_2O_2-generating method to leverage OleT_{SA} catalysis.

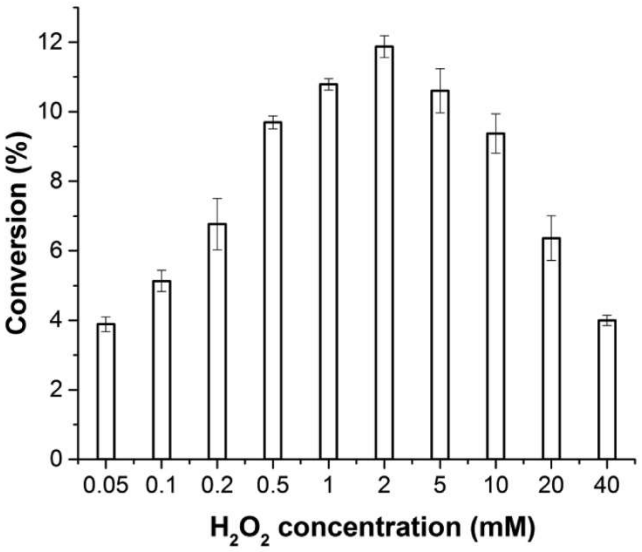

Fig. 2. The H_2O_2 concentration dependence of OleT_{SA} enzyme activity. Reaction condition: 5 μM OleT_{SA}, 1 mM eicosanoic acid, 0.05 mM–40 mM H_2O_2, room temperature for 30 min. Error bars indicate the standard deviation of two independent experiments (n = 2).

3.2. Effect of different GOx substrates on the enzyme cascade catalysis

It has been reported that GOx not only efficiently oxidizes D-glucose but also consumes different sugars including D-mannose, D-galactose and D-xylose among others with slower reaction rates (Gibson et al., 1964; Singh and Verma, 2013), which provides a useful method to tune the rate of H_2O_2-generation to better optimize OleT catalysis. To maximize the potential of a multi-enzyme system, kinetic matching of each enzymatic reaction is important (Dvorak et al., 2014). In order to optimize the stoichiometry of GOx and OleT_{SA} in the tandem catalysis reaction, different concentrations of GOx were tested with fixed concentrations of OleT_{SA} and varying sugar substrates. As shown in Fig. 3**a**, with glucose as a substrate, 10 nM GOx (0.002 M equivalents to OleT_{SA}) leads to maximized substrate conversion. Upon increasing the GOx concentration further, the product yield decreased, which could be caused by enzyme inactivation due to excess H_2O_2 produced from the GOx/glucose reaction. When mannose or galactose was used, at least one molar equivalent of GOx to OleT_{SA} was needed to maximize the conversion rate. A similar phenomenon was observed in the assay where hydrocinnamic acid was metabolized by OleT_{SA} to produce styrene. However, it is noteworthy that upon increasing the mannose concentration up to 13 mM, styrene production continued to rise (a ~30–50% increase, depending on the different GOx concentration).

A typical time course of product formation with the optimized GOx/OleT ratio is shown in Fig. 3**b**. Decarboxylation continues to proceed until the end of the test (2 h) in the GOx method, demonstrating clear advantages of enzyme utility by comparing with that in the H_2O_2 method. As a control, a glucose titration test with GOx method shows increasing OleT_{SA} activity with increasing glucose concentration, while with H_2O_2 method, glucose had no such effect, indicating that the enhancement of activity by glucose only occurs when paired with GOx. It is apparent that controlling the *in situ* H_2O_2-generation rate to maintain an appropriate H_2O_2 level during OleT_{SA} catalysis is important to maximize its enzymatic conversion. In summary, the GOx method shows significantly improved OleT_{SA} catalytic efficiency than the H_2O_2 method, while GOx enzyme pairing with different sugars makes the method flexible to leverage OleT enzyme catalysis. Based on this, we demonstrated the kinetic matching of the tandem catalysis may be an important parameter to optimize the enzyme cascade efficiency.

3.3. GOx/OleT_{SA} enzyme cascade catalysis test with different fatty acids

Abundant and bioavailable fatty acids provide a renewable source for the sustainable production of terminal alkenes. How to improve conversion yield has been a major pursuit for the OleT enzyme's application (Lu et al., 2018; Matthews et al., 2017). Here, we tested the GOx/OleT_{SA} enzyme cascade activity with a selection of fatty acids including eicosanoic acid, stearic acid, palmitic acid, myristic acid and lauric acid using glucose as a GOx substrate at the optimized condition

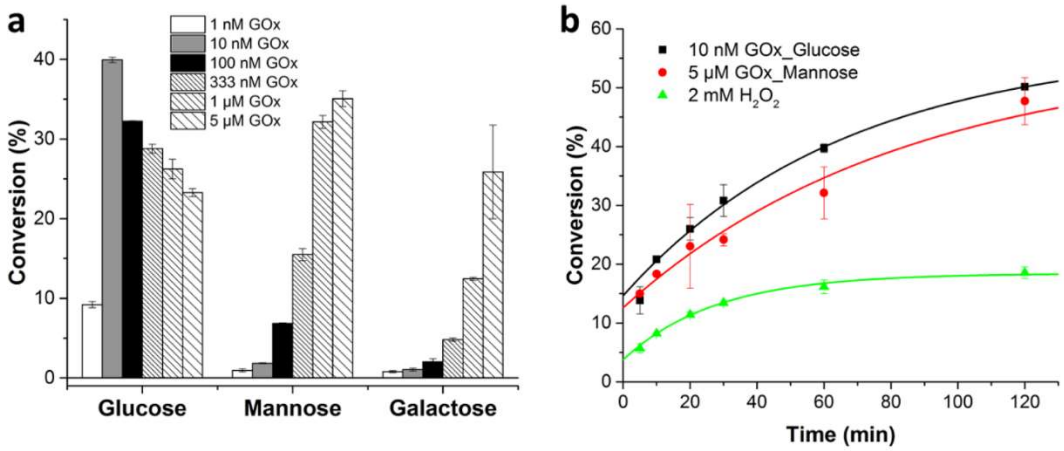

Fig. 3. $OleT_{SA}$ catalysis can be driven by different sugars with optimized GOx enzyme concentration. (a) Comparison of the conversion of eicosanoic acid with the $OleT_{SA}$/GOx catalysis in a 60 min reaction time. (b) A time course comparison with GOx_Glucose and GOx_Mannose as H_2O_2 source vs. direct addition of H_2O_2 (2 mM). An exponential model was used to fit the data in (b). Reaction conditions were as follows: 5 μM $OleT_{SA}$, 6.6 mM sugars, 1 mM eicosanoic acid, GOx (concentrations as indicated) at room temperature. Error bars indicate the standard deviation of duplicate experiments (n = 2).

Table 1
$OleT_{SA}$ metabolic profile with different FAs with either the GOx or H_2O_2 method.

Substrate	Method	Alkene (%)	Alcohol (%)	Conv. (%)
eicosanoic acid	GOx	> 99	NA	50 ± 5
	H_2O_2	> 99	NA	12 ± 2
stearic acid	GOx	> 99	< 1	71 ± 3
	H_2O_2	> 99	< 1	57 ± 1
palmitic acid	GOx	62	38	93 ± 7
	H_2O_2	49	51	23 ± 4
myristic acid	GOx	63	37	99 ± 3
	H_2O_2	60	40	75 ± 5
lauric acid	GOx	59	41	92 ± 7
	H_2O_2	50	50	71 ± 5

Reaction conditions: 5 μM $OleT_{SA}$, 0.5 mM fatty acid substrate, and either 0.01 μM GOx with 6.6 mM glucose or 2 mM H_2O_2. The reaction was in a total volume of 300 μL and carried out at room temperature for 60 min.

Table 2
$OleT_{SA}$ metabolism profile with different FAs with GOx and H_2O_2 method for overnight reactions.

Substrate	Method	Alkene (%)	Alcohol (%)	Conv. (%)
eicosanoic acid	GOx	> 99%	NA	> 99%
	H_2O_2	> 99%	NA	13 ± 4
stearic acid	GOx	> 99%	< 1%	35 ± 2
	H_2O_2	> 99%	< 1%	3 ± 1
palmitic acid	GOx	63	37	94 ± 3
	H_2O_2	41	59	35 ± 1
myristic acid	GOx	79	21	> 99%
	H_2O_2	60	40	81 ± 3
lauric acid	GOx	74	26	> 99%
	H_2O_2	47	53	75 ± 13

Reaction conditions: $OleT_{SA}$ 5 μM, substrate 0.5 mM, GOx 0.01 μM, glucose 6.6 mM or H_2O_2 2 mM, 300 μL reaction at room temperature for overnight.

(molar ratio of GOx:$OleT_{SA}$ = 1:500) as described above. By comparison to the one-time H_2O_2 injection method, GOx method exhibits 25% to 300% higher conversion of substrate to product depending on the fatty acid substrate used (Table 1). With long-term reactions, the GOx method showed further increased substrates conversion, while there was no improvement with time in the H_2O_2 method, which supports our hypothesis the function of $OleT_{SA}$ is irreversibly hampered by a one-time injection of H_2O_2 (Table 2). The chemo-specificity of enzymatic catalysis was similar in both two methods (Table 3).

Table 3
$OleT_{SA}$ metabolized alcohol products profile comparison with the GOx method[a] and H_2O_2 method[b].

Substrate	Method	Alcohol (%)
eicosanoic acid	GOx	NA
	H_2O_2	NA
stearic acid	GOx	< 1%
	H_2O_2	< 1%
palmitic acid	GOx	8% α, 63% β, 29% γ
	H_2O_2	3% α, 97% β, NA γ
myristic acid	GOx	26% α, 75% β, NA γ
	H_2O_2	19% α, 81% β, NA γ
lauric acid	GOx	11% α, 73% β, 16% γ
	H_2O_2	4% α, 96% β, NA γ

Note: The different alcohols (α-, β-, γ-) were identified by GC/MS fragmentation patterns of derivatized (di-silylated) hydroxy-fatty acid (Amaya, 2018).

[a] Reaction conditions: $OleT_{SA}$ 5 μM, FAs 500 μM, 10 nM GOx, 6.6 mM glucose for 1 h. Alcohol products distribution was calculated based on the according peak areas.

[b] Reaction conditions: $OleT_{SA}$ 5 μM, FAs 500 μM. 5 mM H_2O_2 was perfused with pump within 2 h. The Cβ regiospecificity is defined as the fractional percentage of alkenes and Cβ alcohols over total products formed by the enzyme.

3.4. Heme destruction is prevented using the GOx method of H_2O_2 addition

The improved $OleT_{SA}$ enzyme catalytic activity with GOx method was attributed to a gradual and robust production of H_2O_2 that prevents heme degradation during the tandem catalysis. To confirm this hypothesis, $OleT_{SA}$ spectra were monitored during the enzymatic reactions with either one-time H_2O_2 addition or the gradual introduction using GOx (Fig. 4**a and b**). The Soret peak was used as a handle for monitoring heme integrity. As expected, $OleT_{SA}$ enzyme shifts from the high-spin (substrate-bound) state to the low-spin (substrate-free/product-bound) state spontaneously upon treatment with 2 mM H_2O_2, and stays predominantly in this state for the remainder of the time course test. We have previously determined in $OleT_{JE}$ that product release is significantly slower than the chemical steps (e.g·H_2O_2 activation, C–H abstraction) that lead to alkene generation (Amaya et al., 2018), consistent with the spectra obtained here. Within minutes, the heme chromophore bleaches during the H_2O_2 treatment. On the other hand, with the GOx method, the low-spin Soret maximum at 418 nm appears after 5 min of reaction, indicating most of the proteins are substrate-free/product-bound like that of the H_2O_2 method, which suggests there is a burst of H_2O_2 during this period. Then, the enzyme returns back to

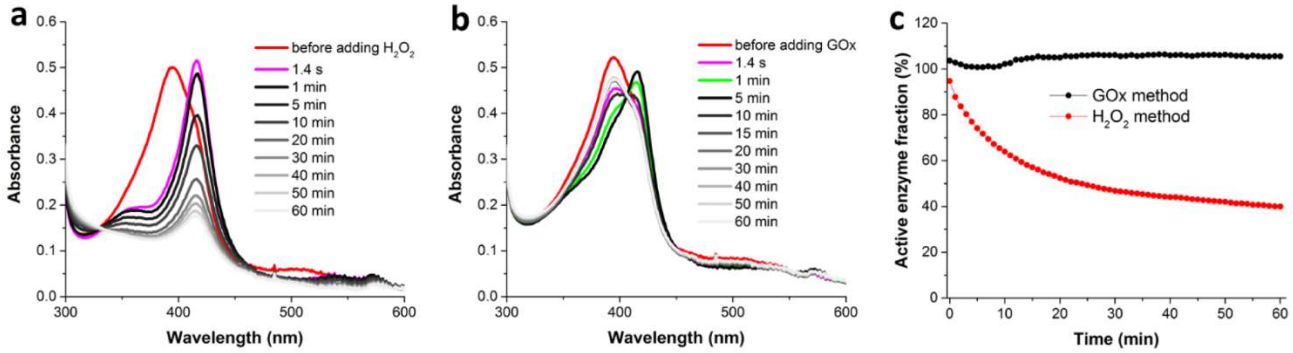

Fig. 4. Soret band monitoring during $OleT_{SA}$ catalytic reactions with H_2O_2 method (a) and GOx method (b). In all reactions, 5 μM $OleT_{SA}$, 0.5 mM eicosanoic acid, 2 mM H_2O_2 or 10 nM GOx, 6.6 mM glucose were used. (c) Active $OleT_{SA}$ enzyme fraction comparison during the catalytic reactions with GOx and H_2O_2 methods.

predominantly high-spin state for the remainder of the assay. This indicates that the majority of the $OleT_{SA}$ is in the substrate-bound state and that H_2O_2 production by GOx is now rate-limiting. The sluggishness of peroxide generation protects the heme from H_2O_2-mediated degradation to afford the higher overall turnover numbers shown above. As quantitative confirmation, the Soret peak intensity (as the sum of high-spin and low-spin) was used to determine the fraction of active enzyme throughout the time course study. As shown in Fig. 4**c**, more than half of the enzyme was inactivated within 1 h in the H_2O_2 method, whereas with the GOx method, the amount of active $OleT_{SA}$ enzyme remained unchanged after 1 h, which is consistent with the observation that $OleT_{SA}$ is continually active during this time period (Fig. 3b). We rationalize that the GOx-based *in situ* H_2O_2-generation method maintains H_2O_2 concentrations at a level compatible with OleT catalysis while minimizing the heme destruction during the catalysis. By comparing different methods used for the OleT enzymatic reaction in previous studies, our method provides a simple and efficient way to improve the enzyme catalysis.

3.5. Polymer-GOx-$OleT_{SA}$ assembly to improve enzyme cascade catalytic efficiency

Inspired by natural multienzyme complexes that exhibit extraordinary efficiency (Liang and Anderson, 1998), a variety of enzyme cascades have recently been developed via co-localization of enzymes on nanostructured scaffolds (Delebecque et al., 2011; Dueber et al., 2009; Xu et al., 2019) to enable cooperative catalytic mechanisms such as facilitating intermediate transportation (Fu et al., 2012; Haga et al., 2018), kinetic modification via enzyme or intermediate substrate scaffold interactions (Fu et al., 2012), stoichiometry optimization (Dueber et al., 2009; Xu et al., 2019), and encapsulation (Chen et al., 2018), etc. We therefore attempted to co-assemble GOx/$OleT_{SA}$ enzyme pairs on a polymeric support to further promote enzymatic catalysis. In our previous studies, we used P4VP and other polymers to co-assemble different proteins to generate core–shell nanoparticles (NPs) and demonstrated a high protein loading capacity and a close proximity of the proteins on the surface of the NPs (Lu et al., 2019; Suthiwangcharoen et al., 2014). Both the fine balance between hydrophobicity and hydrophilicity as well as the hydrogen bonding between proteins and polymers provide a benign environment for proteins to maintain function. Herein, we use this strategy to co-assemble GOx and $OleT_{SA}$ enzymes (Fig. 5**a-b**) in order to improve the enzyme cascade catalytic efficiency. With the assumption that the two enzymes have equal chance to attach to the NPs' surface, equal molar concentration of GOx and $OleT_{SA}$ (1 μM/each enzyme) was used for the co-assembly. TEM and DLS analysis shows successfully assembled polymer-dual-enzymes NP_S with an average size of ~385 nm. For tandem catalytic reactions, mannose was fed, and hydrocinnamic acid or myristic acid was used as an $OleT_{SA}$ substrate to compare the activity of the assemblies to enzymes in solution. $OleT_{SA}$ showed relative low activity on hydrocinnamic acid compared to fatty acid substrates, so 2 mM hydrocinnamic acid was used in the reactions. As shown in Fig. 5**c**, P4VP-GOx-$OleT_{SA}$ assemblies exhibit around 35–40% higher activity than the free GOx/$OleT_{SA}$ in a 60-min reaction at room temperature with different $OleT_{SA}$ substrates. As a control, the mixture of P4VP-GOx and P4VP-$OleT_{SA}$ assemblies showed comparable activity with the free enzymes. Moreover, with dilutions, the co-assembled samples showed further enhanced activity compared to the free enzymes (Fig. 5**d**, ~60% enhanced activity was observed with 5× times dilution of each sample). These results suggest that improved activity of the co-assemblies is related to the close space of enzymes because of the co-localization on the NPs. In addition, if H_2O_2 instead of mannose was used to drive the catalysis, P4VP-GOx-$OleT_{SA}$ did not exhibit any enhanced activity comparing to the free enzymes.

To further test whether the activity enhancement is due to proximity effects, catalase, a scavenger of H_2O_2, was used to challenge the tandem catalysis. As shown in Fig. 5**e**, the reactions catalyzed by P4VP-GOx-$OleT_{SA}$ was much less inhibited by catalase than that of free enzymes. For example, when 250 nM of catalase was included in the reactions, P4VP-GOx-$OleT_{SA}$ still showed ~30% activity, while only 15% activity was observed for free enzymes. This result suggests that on the surface of NP assemblies, some H_2O_2 produced by GOx is transferred to $OleT_{SA}$ directly and is not freely defused into the bulk solution due to the closed proximity of the enzymes. We rationalize that in this system, large amount of enzyme pairs assembled on the nanoparticles surface may provide multiple local targets for H_2O_2 (Idan and Hess, 2013). Moreover, the very closed distance of the enzymes may create a hydration layer (Bagchi, 2005) on the surface of NPs, which facilitates H_2O_2 transportation among enzymes (Fu et al., 2012), making a high local concentration of H_2O_2 around the OleT enzymes. All these factors may contribute to the enhanced GOx/$OleT_{SA}$ enzymatic activity when adhered to NPs' surfaces. However, the only modest activity improvement and slight sensitivity to catalase suggest the assembly is unable to directly tunnel H_2O_2 (Fig. 5b), which could be the reason why there is only a relatively weak enhancement compared to other encapsulation systems (Tan et al., 2017). Nevertheless, the combination of the GOx-driven $OleT_{SA}$ catalysis and the co-localization of the enzyme pairs on polymeric NPs through co-assembly demonstrated an efficient way to improve the cascade enzymatic catalysis. Notably glucose is much cheaper than mannose and more accessible (e.g. from different bioprocesses) in the practical synthesis. A further optimization of the ratio of GOx and OleT in the co-assembly process with supporting polymers may lead to an improved activity with glucose as the energy feed. In addition, the polymer-GOx/$OleT_{SA}$ NPs generated in this system can be easily adapted in the flow reaction systems, in which the substrate concentration, oxygen supply, pH control and product purification could be readily manipulated, providing a potential platform for biofuel production applications.

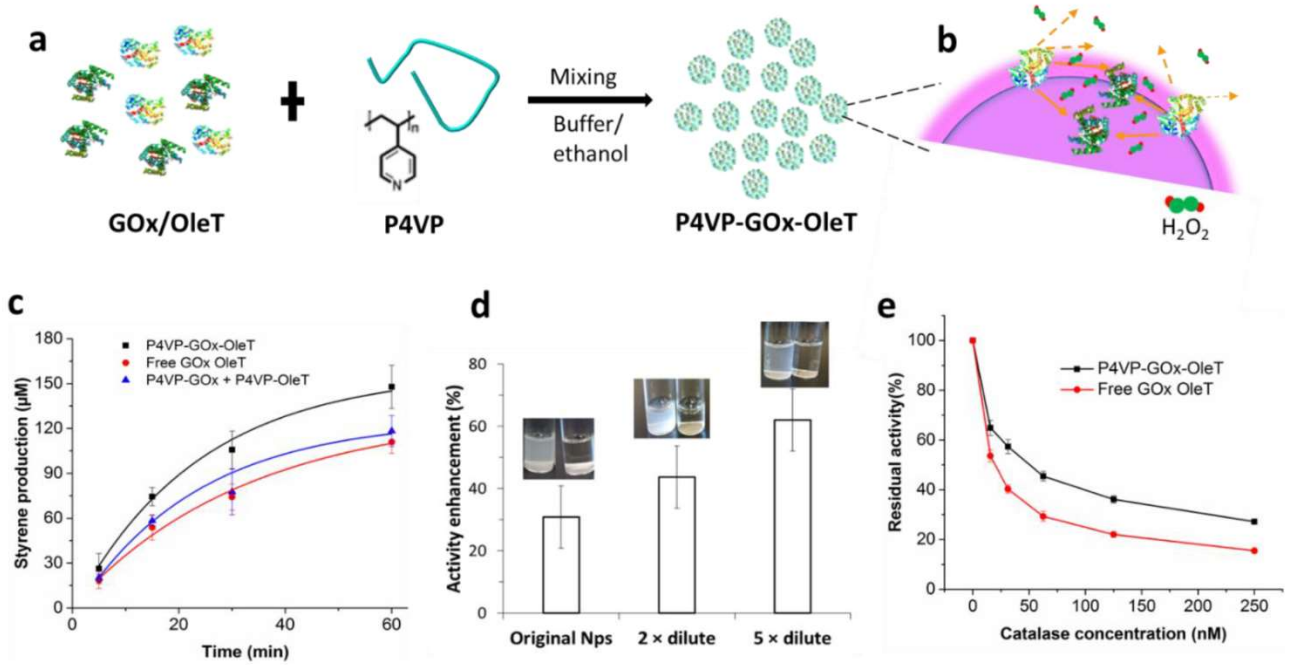

Fig. 5. (a) Schematic illustration of the preparation of P4VP-GOx-OleT_{SA} in buffer/ethanol co-solvent. (b) model of H_2O_2 diffusion on the surface of P4VP-GOx-OleT_{SA} assemblies. The pink color represents hydration layer on the NPs surface (c) P4VP-GOx-OleT_{SA} assemblies show enhanced activity relative to the free enzyme cascade for styrene production with 6.6 mM mannose as sugar source, and 2 mM hydrocinnamic acid as the substrate. An exponential model was used to fit the data. (d) Inhibition effect of catalase on the reactions catalyzed by P4VP-GOx-OleT_{SA} and free GOx/OleT_{SA} mixtures. The reaction condition was the same as in (c) and were quenched after 60 min incubation. Error bars indicate the standard deviation of duplicate experiments (n = 2). (For interpretation of the references to color in this figure legend, the reader is referred to the web version of this article.)

4. Conclusion

In this study, we report the use of a GOx enzyme-based *in situ* H_2O_2-generating method to drive OleT_{SA} catalysis to produce terminal alkenes with significantly improved efficiency than the peroxide method. By adjusting the GOx/OleT_{SA} ratio and using different sugars, our system provides a flexible method to tune the H_2O_2-generating process and thus to leverage the catalysis of OleT_{SA}. With this model, a facile P4VP polymer-dual enzyme co-assembly was developed to further optimize the enzyme cascade catalytic efficiency through enzyme co-localization representing a simple and efficient strategy to transform bioavailable feed stocks such as fatty acids to industrially important chemicals.

CRediT authorship contribution statement

Libo Zhang: Methodology, Data curation, Formal analysis, Writing - original draft. **Olivia M. Manley:** Investigation, Writing - review & editing. **Dumei Ma:** Writing - review & editing, Visualization. **Yingwu Yin:** Investigation. **Thomas M. Makris:** Investigation, Writing - review & editing, Funding acquisition. **Qian Wang:** Conceptualization, Supervision, Project administration, Writing - review & editing, Funding acquisition.

Declaration of Competing Interest

The authors declare that they have no known competing financial interests or personal relationships that could have appeared to influence the work reported in this paper.

Acknowledgement

This work is supported by the ASPIRE grant from the University of South Carolina (TM and QW) and NSF CAREER 1555066 (TM). QW and LZ also acknowledge the support from the NSF and SC EPSCoR/IDeA Program under NSF Award #OIA-1655740. The views, perspective, and content do not necessarily represent the official views of the SC EPSCoR/IDeA Program nor those of the NSF. DM acknowledges support (201806310084) from the State Scholarship Fund of the China Scholarship Council. We also acknowledge support from the staffs at the Mass Spectrometry center at the University of South Carolina.

Appendix A. Supplementary data

Supplementary data to this article can be found online at https://doi.org/10.1016/j.biortech.2020.123538.

References

Adams, E.C., Mast, R.L., Free, A.H., 1960. Specificity of glucose oxidase. Arch. Biochem. Biophys. 91, 230–234. https://doi.org/10.1016/0003-9861(60)90495-1.

Amaya, J.A., Rutland, C.D., Makris, T.M., 2016. Mixed regiospecificity compromises alkene synthesis by a cytochrome P450 peroxygenase from Methylobacterium populi. J. Inorg. Biochem., in: 5th Georgian Bay International Conference on Bioinorganic Chemistry 158, 11–16. DOI:10.1016/j.jinorgbio.2016.02.031.

Amaya, J.A., Rutland, C.D., Leschinsky, N., Makris, T.M., 2018. A distal loop controls product release and chemo- and regioselectivity in cytochrome P450 decarboxylases. Biochemistry 57, 344–353. https://doi.org/10.1021/acs.biochem.7b01065.

Amaya, J., 2018. Mechanisms of Decarboxylation in The CYP152 Family of Cytochrome P450S. Theses Diss.

Aransiola, E.F., Ojumu, T.V., Oyekola, O.O., Madzimbamuto, T.F., Ikhu-Omoregbe, D.I.O., 2014. A review of current technology for biodiesel production: state of the art. Biomass Bioenergy 61, 276–297. https://doi.org/10.1016/j.biombioe.2013.11.014.

Ayala, M., Batista, C.V., Vazquez-Duhalt, R., 2011. Heme destruction, the main molecular event during the peroxide-mediated inactivation of chloroperoxidase from Caldariomyces fumago. J. Biol. Inorg. Chem. JBIC Publ. Soc. Biol. Inorg. Chem. 16, 63–68. https://doi.org/10.1007/s00775-010-0702-6.

Bagchi, B., 2005. Water dynamics in the hydration layer around proteins and micelles. Chem. Rev. 105, 3197–3219. https://doi.org/10.1021/cr020661+.

Bankar, S.B., Bule, M.V., Singhal, R.S., Ananthanarayan, L., 2009. Glucose oxidase — an overview. Biotechnol. Adv. 27, 489–501. https://doi.org/10.1016/j.biotechadv.2009.04.003.

Bhatia, S.K., Gurav, R., Choi, T.-R., Jung, H.-R., Yang, S.-Y., Moon, Y.-M., Song, H.-S., Jeon, J.-M., Choi, K.-Y., Yang, Y.-H., 2019. Bioconversion of plant biomass

hydrolysate into bioplastic (polyhydroxyalkanoates) using Ralstonia eutropha 5119. Bioresour. Technol. 271, 306–315. https://doi.org/10.1016/j.biortech.2018.09.122.
Burek, B.O., Bormann, S., Hollmann, F., Bloh, J.Z., Holtmann, D., 2019. Hydrogen peroxide driven biocatalysis. Green Chem. 21, 3232–3249. https://doi.org/10.1039/C9GC00633H.
Chen, W.-H., Vázquez-González, M., Zoabi, A., Abu-Reziq, R., Willner, I., 2018. Biocatalytic cascades driven by enzymes encapsulated in metal–organic framework nanoparticles. Nat. Catal. 1, 689. https://doi.org/10.1038/s41929-018-0117-2.
Corma, A., Iborra, S., Velty, A., 2007. Chemical routes for the transformation of biomass into chemicals. Chem. Rev. 107, 2411–2502. https://doi.org/10.1021/cr050989d.
Das, S., Join, B., Junge, K., Beller, M., 2012. A general and selective copper-catalyzed reduction of secondary amides. Chem. Commun. 48, 2683–2685. https://doi.org/10.1039/C2CC17209G.
Delebecque, C.J., Lindner, A.B., Silver, P.A., Aldaye, F.A., 2011. Organization of intracellular reactions with rationally designed RNA assemblies. Science 333, 470–474. https://doi.org/10.1126/science.1206938.
Dennig, A., Kurakin, S., Kuhn, M., Dordic, A., Hall, M., Faber, K., 2016. Enzymatic oxidative tandem decarboxylation of dioic acids to terminal dienes. Eur. J. Org. Chem. 2016, 3473–3477. https://doi.org/10.1002/ejoc.201600358.
Dueber, J.E., Wu, G.C., Malmirchegini, G.R., Moon, T.S., Petzold, C.J., Ullal, A.V., Prather, K.L.J., Keasling, J.D., 2009. Synthetic protein scaffolds provide modular control over metabolic flux. Nat. Biotechnol. 27, 753–759. https://doi.org/10.1038/nbt.1557.
Dvorak, P., Kurumbang, N.P., Bendl, J., Brezovsky, J., Prokop, Z., Damborsky, J., 2014. Maximizing the efficiency of multienzyme process by stoichiometry optimization. ChemBioChem 15, 1891–1895. https://doi.org/10.1002/cbic.201402265.
Fu, J., Liu, M., Liu, Y., Woodbury, N.W., Yan, H., 2012. Interenzyme substrate diffusion for an enzyme cascade organized on spatially addressable DNA nanostructures. J. Am. Chem. Soc. 134, 5516–5519. https://doi.org/10.1021/ja300897h.
Gibson, Q.H., Swoboda, B.E., Massey, V., 1964. Kinetics and mechanism of action of glucose oxidase. J. Biol. Chem. 239, 3927–3934. https://www.jbc.org/content/239/11/3927.full.pdf.
Grant, J.L., Hsieh, C.H., Makris, T.M., 2015. Decarboxylation of fatty acids to terminal alkenes by cytochrome P450 compound I. J. Am. Chem. Soc. 137, 4940–4943. https://doi.org/10.1021/jacs.5b01965.
Grant, J.L., Mitchell, M.E., Makris, T.M., 2016. Catalytic strategy for carbon – carbon bond scission by the cytochrome P450 OleT. Proc. Natl. Acad. Sci. 113, 10049–10054. https://doi.org/10.1073/pnas.1606294113.
Haga, T., Hirakawa, H., Nagamune, T., 2018. Artificial self-sufficient cytochrome P450 containing multiple auxiliary proteins demonstrates improved monooxygenase activity. Biotechnol. J. 13, 1800088. https://doi.org/10.1002/biot.201800088.
Idan, O., Hess, H., 2013. Origins of activity enhancement in enzyme cascades on scaffolds. ACS Nano 7, 8658–8665. https://doi.org/10.1021/nn402823k.
Jiang, Y., Li, Z., Wang, C., Zhou, Y.J., Xu, H., Li, S., 2019. Biochemical characterization of three new α-olefin-producing P450 fatty acid decarboxylases with a halophilic property. Biotechnol. Biofuels 12, 79. https://doi.org/10.1186/s13068-019-1419-6.
Joo, H., Lin, Z., Arnold, F.H., 1999. Laboratory evolution of peroxide-mediated cytochrome P450 hydroxylation. Nature 399, 670–673. https://doi.org/10.1038/21395.
Karich, A., Scheibner, K., Ullrich, R., Hofrichter, M., 2016. Exploring the catalase activity of unspecific peroxygenases and the mechanism of peroxide-dependent heme destruction. J. Mol. Catal. B Enzyme. 134, 238–246. https://doi.org/10.1016/j.molcatb.2016.10.014.
Karuzina, I.I., Archakov, A.I., 1994. Hydrogen peroxide-mediated inactivation of microsomal cytochrome P450 during monooxygenase reactions. Free Radic. Biol. Med. 17, 557–567. https://doi.org/10.1016/0891-5849(94)90095-7.
Lane, B.S., Burgess, K., 2001. A cheap, catalytic, scalable, and environmentally benign method for alkene epoxidations. J. Am. Chem. Soc. 123, 2933–2934. https://doi.org/10.1021/ja004000a.
Liang, P.-H., Anderson, K.S., 1998. Substrate channeling and domain – domain interactions in bifunctional thymidylate synthase – dihydrofolate reductase. Biochemistry 37, 12195–12205. https://doi.org/10.1021/bi9803168.
Liu, Y., Wang, C., Yan, J., Zhang, W., Guan, W., Lu, X., Li, S., 2014. Hydrogen peroxide-independent production of α-alkenes by OleTJE P450 fatty acid decarboxylase. Biotechnol. Biofuels 7, 28. https://doi.org/10.1186/1754-6834-7-28.
Lu, C., Shen, F., Wang, S., Wang, Y., Liu, J., Bai, W.-J., Wang, X., 2018. An engineered self-sufficient biocatalyst enables scalable production of linear α-olefins from carboxylic acids. ACS Catal. 8, 5794–5798. https://doi.org/10.1021/acscatal.8b01313.
Lu, L., Zhang, L., Yuan, L., Zhu, T., Chen, W., Wang, G., Wang, Q., 2019. Artificial cellulosome complex from the self-assembly of Ni-NTA-functionalized polymeric micelles and cellulases. ChemBioChem 20, 1394–1399. https://doi.org/10.1002/cbic.201900061.
Mateo, W., Lei, H., Villota, E., Qian, M., Zhao, Y., Huo, E., Zhang, Q., Lin, X., Wang, C., Huang, Z., 2020. Synthesis and characterization of sulfonated activated carbon as a catalyst for bio-jet fuel production from biomass and waste plastics. Bioresour. Technol. 297, 122411. https://doi.org/10.1016/j.biortech.2019.122411.
Matthews, S., Tee, K.L., Rattray, N.J., McLean, K.J., Leys, D., Parker, D.A., Blankley, R.T., Munro, A.W., 2017. Production of alkenes and novel secondary products by P450 OleTJE using novel H2 O2 -generating fusion protein systems. FEBS Lett. 591, 737–750. https://doi.org/10.1002/1873-3468.12581.
Munro, A.W., McLean, K.J., Grant, J.L., Makris, T.M., 2018. Structure and function of the cytochrome P450 peroxygenase enzymes. Biochem. Soc. Trans. BST20170218. https://doi.org/10.1042/BST20170218.
Ogola, H.J.O., Hashimoto, N., Miyabe, S., Ashida, H., Ishikawa, T., Shibata, H., Sawa, Y., 2010. Enhancement of hydrogen peroxide stability of a novel Anabaena sp. DyP-type peroxidase by site-directed mutagenesis of methionine residues. Appl. Microbiol. Biotechnol. 87, 1727–1736. https://doi.org/10.1007/s00253-010-2603-6.
Peralta-Yahya, P.P., Zhang, F., del Cardayre, S.B., Keasling, J.D., 2012. Microbial engineering for the production of advanced biofuels. Nature 488, 320–328. https://doi.org/10.1038/nature11478.
Potocnik, J., 2007. Renewable energy sources and the realities of setting an energy agenda. Science 315, 810–811. https://doi.org/10.1126/science.1139086.
Ray, S., Rao, P.V.C., Choudary, N.V., 2012. Poly-α-olefin-based synthetic lubricants: a short review on various synthetic routes. Lubr. Sci. 24, 23–44. https://doi.org/10.1002/ls.166.
Rude, M.A., Baron, T.S., Brubaker, S., Alibhai, M., Cardayre, S.B.D., Schirmer, A., 2011. Terminal olefin (1-Alkene) Biosynthesis by a Novel P450 fatty acid decarboxylase from jeotgalicoccus species. Appl. Env. Microbiol. 77, 1718–1727. https://doi.org/10.1128/AEM.02580-10.
Singh, J., Verma, N.S., 2013. Glucose oxidase from Aspergillus niger: production, characterization and immobilization for glucose oxidation. Adv. Appl. Sci. Res. 4, 250–257. https://www.imedpub.com/articles/glucose-oxidase-from-aspergillus-nigerproduction-characterization-and-immobilization-for-glucose-oxidation.pdf.
Suthiwangcharoen, N., Li, T., Wu, L., Reno, H.B., Thompson, P., Wang, Q., 2014. Facile co-assembly process to generate core-shell nanoparticles with functional protein corona. Biomacromolecules 15, 948–956. https://doi.org/10.1021/bm401819x.
Tan, H., Guo, S., Dinh, N.-D., Luo, R., Jin, L., Chen, C.-H., 2017. Heterogeneous multicompartmental hydrogel particles as synthetic cells for incompatible tandem reactions. Nat. Commun. 8, 663. https://doi.org/10.1038/s41467-017-00757-4.
Vidal-Limón, A., Águila, S., Ayala, M., Batista, C.V., Vazquez-Duhalt, R., 2013. Peroxidase activity stabilization of cytochrome P450BM3 by rational analysis of intramolecular electron transfer. J. Inorg. Biochem. 122, 18–26. https://doi.org/10.1016/j.jinorgbio.2013.01.009.
Wilson, R., Turner, A.P.F., 1992. Glucose oxidase: an ideal enzyme. Biosens. Bioelectron. 7, 165–185. https://doi.org/10.1016/0956-5663(92)87013-F.
Wise, C.E., Hsieh, C.H., Poplin, N.L., Makris, T.M., 2018. Dioxygen activation by the biofuel-generating cytochrome P450 OleT. ACS Catal. 8, 9342–9352. https://doi.org/10.1021/acscatal.8b02631.
Xu, C., Zhang, J., Zhang, Y., Guo, Y., Xu, H., Xu, J., Wang, Z., 2019. Enhancement of high-solids enzymatic hydrolysis efficiency of alkali pretreated sugarcane bagasse at low cellulase dosage by fed-batch strategy based on optimized accessory enzymes and additives. Bioresour. Technol. 292, 121993. https://doi.org/10.1016/j.biortech.2019.121993.
Zachos, I., Gaßmeyer, S.K., Bauer, D., Sieber, V., Hollmann, F., Kourist, R., 2015. Photobiocatalytic decarboxylation for olefin synthesis. Chem. Commun. 51, 1918–1921. https://doi.org/10.1039/C4CC07276F.